Modified full abundance-constrained spectral unmixing

Englin Wong, Chein-I Chang

Englin Wong, Chein-I Chang, "Modified full abundance-constrained spectral unmixing," Proc. SPIE 8539, High-Performance Computing in Remote Sensing II, 85390F (24 October 2012); doi: 10.1117/12.979187

SPIE.

Event: SPIE Remote Sensing, 2012, Edinburgh, United Kingdom

Modified Fully Abundance-Constrained Spectral Unmixing

Englin Wong and Chein-I Chang

Remote Sensing Signal and Image Processing Laboratory
Department of Computer Science and Electrical Engineering
University of Maryland, Baltimore County, Baltimore, MD 21250

Abstract

Abundance fully constrained least squares (FLCS) method has been widely used for spectral unmixing. A modified FCLS (MFCLS) was previously proposed for the same purpose to derive two iterative equations for solving fully abundance-constrained spectral unmixing problems. Unfortunately, its advantages have not been recognized. This paper conducts a comparative study and analysis between FCLS and MFCLS via custom-designed synthetic images and real images to demonstrate that while both methods perform comparably in unmixing data, MFCLS edges out FCLS in less computing time.

Keywords: Fully constrained least squares (FLCS). Modified fully constrained least squares (MFLCS). Spectral unmixing.

1. INTRODUCTION

Fully constrained least squares (FCLS) method has been widely used spectral unmixing technique to unmix data samples in terms of abundance fractions of image endmembers assumed to b present in the data via a linear mixing model [1-2]. In order to accurately estimate these abundance fractions two abundance constraints, abundance sum-to-one constraint (ASC) and abundance non-negativity constraint (ANC) must be imposed on the used linear mixing model. The FCLS was developed for this purpose. Since the ANC is an inequality constraint, there is no close form can be derived to calculate thgese abundance fractions analytically. As a result, FCLS is indeed a numerical algorithm to find numerical solutions via two iterative equations. An alternative to FCLS was also developed and referred to as modified FCLS (MFCLS) in [2-3] which replaces the inequality of ANC by an equality constraint while also imposing ASC simultaneously. With these two equality constraints imposed on a linear mixing model, MFCLS is able to derive close forms to perform spectral unmixing. Interestingly, MFCLS has received little interest since it was introduced in [2-3]. Two major reasons are attributed to this incident. One is that FCLS has been developed before MFCLS and has shown to be very effective. So, it is expected that no other algorithms can compete against FCLS and its variants. A second reason is that MFCLS has not been publicized in community of spectral unmixing. In this case, very few are aware of its existence and recognize advantage of using MFCLS over FCLS. This paper takes up this issue and conducts a comparative study between these two via synthetic image experiments. Two applications are considered for experiments. One is hyperspectral imaging and the other is magnetic resonance imaging. The experimental results demonstrate that both methods are indeed produced nearly the same quantitative results but MFCLS seems to require significantly less computing time.

2. LINEAR SPECTRAL UNMIXING

In what follows, we briefly describe the LSMA.

LSMA is a widely used technique to unmix multi-component composition in remote sensing imagery. It assumes that a remote sensing image pixel can be linearly mixed by a number of so-called image endmembers assumed to be basic constituents in the image data, denoted by $\mathbf{m}_1, \mathbf{m}_2, \cdots, \mathbf{m}_p$ that are used to form a signature matrix. Let $\mathbf{r}$ be an L-dimensional image pixel vector where L is the number of image pulse sequences used for MR data acquisition and each image acquire by a particular spectral band. The LSMA models $\mathbf{r}$ as a linear mixture described by

$$\mathbf{r} = \mathbf{M}\boldsymbol{\alpha} + \mathbf{n} \tag{1}$$

High-Performance Computing in Remote Sensing II, edited by Bormin Huang, Antonio J. Plaza,
Proc. of SPIE Vol. 8539, 85390F · © 2012 SPIE · CCC code: 0277-786/12/$18
doi: 10.1117/12.979187

where **n** is accounted for noise or model error and $\boldsymbol{\alpha} = (\alpha_1, \alpha_2, \ldots, \alpha_p)^T$ is an unknown p-dimensional abundance vector associated with $\mathbf{m}_1$, $\mathbf{m}_2$, … , $\mathbf{m}_p$ with α_j representing the abundance fraction of the j^{th} signature $\mathbf{m}_j$ present in the pixel vector **r**. Due to physical constraints, two abundance constraints are generally imposed on (1), which are abundance sum-to-one constraint (ASC) specified by $\sum_{j=1}^{p} \alpha_j = 1$ and abundance non-negativity constraint (ANC) specified by $\alpha_j \geq 0$ for all $1 \leq j \leq p$. In other words, the LSMA takes advantage of (1) to unmix the data sample vector **r** via p signatures, $\mathbf{m}_1$, $\mathbf{m}_2$, … , $\mathbf{m}_p$ by finding their respective abundance fractions $\alpha_1, \alpha_2, \cdots, \alpha_p$ with or without the abundance constraints, ASC and ANC.

2.1 Abundance-Unconstrained Least Squares Method

A simple and general approach to solving (1) is to consider (1) as a least squares (LS) problem without any constraint in which makes use of least squares error (LSE)

$$(\mathbf{M}\boldsymbol{\alpha} - \mathbf{r})^T (\mathbf{M}\boldsymbol{\alpha} - \mathbf{r}) \tag{2}$$

to derive the optimal LS solution given by [1]

$$\hat{\boldsymbol{\alpha}}^{\text{LS}}(\mathbf{r}) = \left(\mathbf{M}^T\mathbf{M}\right)^{-1}\mathbf{M}^T\mathbf{r}. \tag{3}$$

Interestingly, it has been shown in [2-5] that the solution $\hat{\boldsymbol{\alpha}}^{\text{LS}}(\mathbf{r})$ given by (3) is identical to a least squares orthogonal subspace projection (LSOSP), $\hat{\boldsymbol{\alpha}}^{\text{LSOSP}}(\mathbf{r})$.

2.2 SCLS

Eq. (1) is a general linear mixture model with no constraints imposed on the abundance vector $\boldsymbol{\alpha} = \left(\alpha_1 \ \alpha_2 \cdots \alpha_p\right)^T$. So, from an abundance quantification's point of view, it does not provide accurate estimates of abundance fractions and only offers a suboptimal solution. In this section, we consider a partially constrained approach by imposing the ASC on (1) that results in the following SCLS linear mixing problem:

$$\min_{\boldsymbol{\alpha}\in\Delta} \left\{(\mathbf{r} - \mathbf{M}\boldsymbol{\alpha})^T(\mathbf{r} - \mathbf{M}\boldsymbol{\alpha})\right\} \text{ subject to } \Delta = \left\{\boldsymbol{\alpha} \mid \textstyle\sum_{J=1}^{p} \alpha_j = 1\right\}. \tag{4}$$

The solution, $\hat{\boldsymbol{\alpha}}^{\text{SCLS}}(\mathbf{r})$ to (4) can be obtained by

$$\hat{\boldsymbol{\alpha}}^{\text{SCLS}}(\mathbf{r}) = P_{\mathbf{M},\mathbf{1}}^{\perp}\hat{\boldsymbol{\alpha}}^{\text{LS}}(\mathbf{r}) + \left(\mathbf{M}^T\mathbf{M}\right)^{-1}\mathbf{1}\left[\mathbf{1}^T\left(\mathbf{M}^T\mathbf{M}\right)^{-1}\mathbf{1}\right]^{-1} \tag{5}$$

where $\hat{\boldsymbol{\alpha}}^{\text{LS}}(\mathbf{r})$ is given by (3) and

$$P_{\mathbf{M},\mathbf{1}}^{\perp} = \mathbf{I} - \left(\mathbf{M}^T\mathbf{M}\right)^{-1}\mathbf{1}\left[\mathbf{1}^T\left(\mathbf{M}^T\mathbf{M}\right)^{-1}\mathbf{1}\right]^{-1} \tag{6}$$

2.3 NCLS

The SCLS developed in 2.2 only imposes ASC without ANC on (1). As an laternative, we can also impose ANC without ASC on (1) which results in the following optimization problem

$$\min_{\boldsymbol{\alpha}}(\mathbf{M}\boldsymbol{\alpha}-\mathbf{r})^T(\mathbf{M}\boldsymbol{\alpha}-\mathbf{r}) \quad \text{subject to} \quad \alpha_j \geq 0 \text{ for all } 1 \leq j \leq p. \tag{7}$$

Using Largrange's multiplier method, we define the following objective function

$$J = \frac{1}{2}(\mathbf{M}\boldsymbol{\alpha}-\mathbf{r})^T(\mathbf{M}\boldsymbol{\alpha}-\mathbf{r}) + \boldsymbol{\lambda}(\boldsymbol{\alpha}-\mathbf{c}) \tag{8}$$

where $\boldsymbol{\lambda} = (\lambda_1, \lambda_2, ..., \lambda_p)^T$ is a Lagrange multiplier vector and a constraint vector $\mathbf{c} = (c_1, c_2, ..., c_p)^T$ with $c_j > 0$ for $1 \leq j \leq p$. By letting $\boldsymbol{\alpha}$ be $\mathbf{c}$ we can derive the abundance-unconstrained least squares estimate of the partial volume vector $\boldsymbol{\alpha}$, denoted by $\hat{\boldsymbol{\alpha}}^{\mathrm{LS}}(\mathbf{r})$, as

$$\hat{\boldsymbol{\alpha}}^{\mathrm{LS}}(\mathbf{r}) = (\mathbf{M}^T\mathbf{M})^{-1}\mathbf{M}^T\mathbf{r} - (\mathbf{M}^T\mathbf{M})^{-1}\boldsymbol{\lambda} \tag{9}$$

Where

$$\boldsymbol{\lambda} = \mathbf{M}^T\mathbf{r} - \mathbf{M}^T\mathbf{M}\hat{\boldsymbol{\alpha}}\ . \tag{10}$$

In order for $\hat{\boldsymbol{\alpha}}^{\mathrm{LS}}(\mathbf{r})$ to further satisfy ANC the following Kuhn-Tucker conditions must be implemented

$$\begin{aligned} &\lambda_i = 0, \quad i \in P \\ &\lambda_i < 0, \quad i \in R \end{aligned} \tag{11}$$

where P and R represent passive and active sets that contain indices representing negative or positive abundances respectfully. By virtue of (8-11) a numerical algorithm, referred to as NCLS can be designed to start off with the initial estimate given by $\hat{\boldsymbol{\alpha}}^{\mathrm{LS}}(\mathbf{r})$ in (3). If all abundance fractions are positive, the NCLS stops. Otherwise, all indices correspond to negative and zero abundance fractions are moved to passive set P and all positive abundance indices are moved to R. According to Kuhn-Tucker conditions (11), any λ_i with index $i \in P$ is set to zero, and other indices are calculated based on (11). If all λ_is are negative, the NCLS stops. If not, the corresponding most negative index is moved from R to P. A new vector $\boldsymbol{\lambda}$ is then recalculated based on the modified index sets and a new Lagrange multiplier vector is further implemented in order to find a new set of abundance fractions. By comparing with index set S, any negative abundance indices are shuffled from P to R. By iteratively implementing (9) and (10) with using $\hat{\boldsymbol{\alpha}}^{\mathrm{LS}}(\mathbf{r})$ in (3) as an initial abundance vector the NCLS can be derived to find an optimal solution to (4), $\hat{\boldsymbol{\alpha}}^{\mathrm{NCLS}}(\mathbf{r})$ [4].

2.4 FCLS

Since NCLS does not impose the ASC, it generated abundance fractions do not necessarily sum up to one. In order to also impose the ASC along with ANC, the FCLS developed in [2] was designed to serve this need. It solves the following constrained optimization problem

$$\begin{aligned} &\min_{\boldsymbol{\alpha}\in\Delta}\left\{(\mathbf{r}-\mathbf{M}\boldsymbol{\alpha})^T(\mathbf{r}-\mathbf{M}\boldsymbol{\alpha})\right\} \quad \text{subject to} \\ &\qquad \Delta = \left\{\alpha \mid \alpha_j \geq 0 \text{ for } \forall j, \sum_{j=1}^{p}\alpha_j = 1\right\}. \end{aligned} \tag{12}$$

The optimal solution to (12) first takes advantage of the LS solution, $\hat{\boldsymbol{\alpha}}^{\mathrm{LS}}$ as an initial estimate to derive

$$\hat{\boldsymbol{\alpha}}^{\mathrm{FCLS}}(\mathbf{r}) = P^{\perp}_{\mathbf{M},\mathbf{1}}\hat{\boldsymbol{\alpha}}^{\mathrm{LS}}(\mathbf{r}) + (\mathbf{M}^T\mathbf{M})^{-1}\mathbf{1}[\mathbf{1}^T(\mathbf{M}^T\mathbf{M})\mathbf{1}]^{-1} \tag{13}$$

And

$$P^{\perp}_{\mathbf{M},\mathbf{1}} = \mathbf{I}_{L\times L} - (\mathbf{M}^T\mathbf{M})^{-1}\mathbf{1}[\mathbf{1}^T(\mathbf{M}^T\mathbf{M})\mathbf{1}]^{-1}\mathbf{1}^T \quad . \tag{14}$$

It then includes ASC together with ANC by introducing a new signature matrix **N** and an observation vector **s** into the NCLS specified by

$$\mathbf{N} = \begin{bmatrix} \eta\mathbf{M} \\ \mathbf{1}^T \end{bmatrix} \text{ and } \mathbf{s} = \begin{bmatrix} \eta\mathbf{r} \\ 1 \end{bmatrix} \tag{15}$$

where η is a parameter to control the effect of ASC on the NCLS and defined as the reciprocal of the maximal element in the matrix $\mathbf{M} = [m_{ij}]$, i.e., $\eta = 1/\max_{ij}\{m_{ij}\}$

3. MFCLS

As mentioned previously, the main difficulty with solving constrained linear mixing problems is the constraint of abundance nonnegativity that prohibits us from using the Lagrange multiplier method to find solutions analytically. In this section, we propose an alternative approach to modify this constraint. Instead of directly dealing with the inequalities, $\alpha_j \geq 0$ for each $1 \leq j \leq p$, we replace them with an absolute abundance sum-to-one constraint (AASC), $\sum_{j=1}^{p}|\alpha_j| = 1$. The advantage of AASC is that the Lagrange multiplier method is now applicable and can be used to derive an iterative algorithm that leads to a desired optimal constrained least squares solution. Additionally, AASC also allows us to exclude negative abundances from solutions. In other words, the only possibility to satisfy both constraints, sum-to-one ($\sum_{j=1}^{p}\alpha_j = 1$) and AASC ($\sum_{j=1}^{p}|\alpha_j| = 1$) is that all the abundances $\{\alpha_j\}_{j=1}^{p}$ must be nonnegative. So, a modified least squares linear mixing problem with constraints, ASC, $\sum_{j=1}^{p}\alpha_j = 1$ and AASC, $\sum_{j=1}^{p}|\alpha_j| = 1$ can be cast as follows.

$$\min_{\boldsymbol{\alpha}\in\boldsymbol{\Delta}}\left\{(\mathbf{r}-\mathbf{M}\boldsymbol{\alpha})^T(\mathbf{r}-\mathbf{M}\boldsymbol{\alpha})\right\} \tag{16}$$

subject to

$$\boldsymbol{\Delta} = \left\{\boldsymbol{\alpha} \mid \sum_{j+1}^{p}\alpha_j = 1 \text{ and } \sum_{j=1}^{p}|\alpha_j| = 1\right\} \tag{17}$$

Using the Largrange multipliers, we can define the following objection function

$$J(\boldsymbol{\alpha}) = (1/2)(\mathbf{r}-\mathbf{M}\boldsymbol{\alpha})^T(\mathbf{r}-\mathbf{M}\boldsymbol{\alpha}) - \lambda_1\left(\sum_{j=1}^{p}\alpha_j - 1\right) - \lambda_1\left(\sum_{j=1}^{p}|\alpha_j| - 1\right) \tag{18}$$

Differentiating (18) with respect to $\boldsymbol{\alpha}$ and setting to zero yields

$$\left.\frac{\partial J(\boldsymbol{\alpha})}{\partial \boldsymbol{\alpha}}\right|_{\hat{\boldsymbol{\alpha}}^{\mathrm{MFCLS}}} = 0 \Rightarrow \hat{\boldsymbol{\alpha}}^{\mathrm{MFCLS}} = \left(\mathbf{M}^T\mathbf{M}\right)^{-1}\left[\mathbf{M}^T\mathbf{r} - \lambda_1\mathbf{1} - \lambda_2 sign(\boldsymbol{\alpha})\right]$$
$$\Rightarrow \hat{\boldsymbol{\alpha}}^{\mathrm{MFCLS}} = \hat{\boldsymbol{\alpha}}^{\mathrm{LS}} - \left(\mathbf{M}^T\mathbf{M}\right)^{-1}\left[\lambda_1\mathbf{1} + \lambda_2 sign(\hat{\boldsymbol{\alpha}}^{\mathrm{LS}})\right] \tag{19}$$

where $\hat{\boldsymbol{\alpha}}^{\mathrm{LS}} = \left(\mathbf{M}^T\mathbf{M}\right)^{-1}\mathbf{M}^T\mathbf{r}$ is the unconstrained least squares estimate of $\boldsymbol{\alpha}$ for (3). We then substitute $\hat{\boldsymbol{\alpha}}_{\mathrm{LS}}$ given by (19) for $\boldsymbol{\alpha}$ in the following constraints

$$\sum_{j=1}^{p}\alpha_j = \mathbf{1}^T\boldsymbol{\alpha} = 1 \tag{20}$$

$$\sum_{j=1}^{p}|\alpha_j| = sign(\boldsymbol{\alpha})^T\boldsymbol{\alpha} = 1 \tag{21}$$

to compute λ_1 and λ_2 where $sign(\boldsymbol{\alpha})$ is a vector given by the sign function of $\boldsymbol{\alpha}$ with the j-th component being the sign of α_j, namely, $sign(\boldsymbol{\alpha}) = (\beta_1, \beta_2, \cdots, \beta_p)^T$ where β_j is defined by

$$\beta_j = \begin{cases} \dfrac{\alpha_j}{|\alpha_j|}; \text{if } \alpha_j \neq 0 \\ 0; \text{if } \alpha_j = 0 \end{cases} \tag{22}$$

The solution to (16-17) can then be obtained by iteratively computing λ_1, λ_2 and $\hat{\boldsymbol{\alpha}}^{\mathrm{MFCLS}}$ using (19-22). The detail of implementing this algorithm is given below.

MFCLS Iterative Algorithm

1. Initialization: Set $\hat{\boldsymbol{\alpha}}^{\mathrm{MFCLS}} = \hat{\boldsymbol{\alpha}}^{\mathrm{SCLS}}$
2. Compute λ_1, λ_2 using (15-18)
3. Compute $\hat{\boldsymbol{\alpha}}^{\mathrm{MFCLS}} = \hat{\boldsymbol{\alpha}}^{\mathrm{SCLS}} - \left(\mathbf{M}^T\mathbf{M}\right)^{-1}\left[\lambda_1\mathbf{1} + \lambda_2 sign(\hat{\boldsymbol{\alpha}}^{\mathrm{MFCLS}})\right]$
4. If there exists one component in $\hat{\boldsymbol{\alpha}}^{\mathrm{MFCLS}}$ which is negative, go to step 2. Otherwise, stop.

It should be noted that in step 1 the algorithm is initialized by taking advantage of the SCLS solution $\hat{\boldsymbol{\alpha}}^{\mathrm{SCLS}}$ in (5). The stopping criterion described in step 4 provides a rule of when the algorithm will be terminated in which case all components must be nonnegative. In general, it requires a fair amount of computation time to reach this requirement. So, in real implementation, we suggest a simpler rule by checking $\sum_{j=1}^{p}|\alpha_j| - 1 < \varepsilon$ for a preselected threshold ε that will guarantee a quick termination.

The purpose of this paper is to document the timing and error processed by FCLS and MFCLS. The main difference between FCLS and MFCLS is their initial constraint conditions. FCLS are constrained with abundance sum-to-one constraint (ASC) and non-negativity constraint by NCLS. Hence, FCLS can be constructed by modifying the desired signature and signature matrix by,

$$\mathbf{N} = \begin{bmatrix} \delta\mathbf{M} \\ \mathbf{1}^T \end{bmatrix} \tag{23}$$

$$\mathbf{s} = \begin{bmatrix} \delta\mathbf{r} \\ \mathbf{1} \end{bmatrix} \tag{24}$$

Then, FCLS algorithm can be dsibed via the NCKS algorithm.

On the other hand, MFCLS uses the absolute value for the constraint of non-negativity. As a result, the algorithm can be seen as follows:

MFCLS Algorithm:

1. Initialization: Set $\mathbf{N} = \begin{bmatrix} \delta\mathbf{M} \\ \mathbf{1}^T \end{bmatrix}$ and $\mathbf{s} = \begin{bmatrix} \delta\mathbf{r} \\ 1 \end{bmatrix}$, where $\delta \approx 1/\max(\max(\mathbf{M}))$.
2. Compute $\hat{\boldsymbol{\alpha}}^{\mathrm{SCLS}}$ using Eq. (2.16) with $\mathbf{N}$ and $\mathbf{s}$. Set $\hat{\boldsymbol{\alpha}}^{(\mathrm{FCLS},0)} = \hat{\boldsymbol{\alpha}}^{\mathrm{SCLS}}$.
3. At the k-th iteration. If all components in $\hat{\boldsymbol{\alpha}}^{(\mathrm{FCLS},k)}$ are positive, the algorithm is terminated. Otherwise, continue.
4. Let $k = k+1$.
5. Move all indices in $P^{(k-1)}$ that correspond to negative components of $\hat{\boldsymbol{\alpha}}^{(\mathrm{FCLS},k-1)}$ to $R^{(k-1)}$ and the resulting index sets are denoted by $P^{(k)}$ and $R^{(k)}$ respectively.
6. Let $\hat{\boldsymbol{\alpha}}_{R^{(k)}}$ denote the vector consisting of all components $\hat{\boldsymbol{\alpha}}^{\mathrm{SCLS}}$ in $R^{(k)}$.
7. Form a steering matrix $\boldsymbol{\Phi}_{\alpha}^{(k)}$ by deleting all rows and columns in the matrix $\left(\mathbf{M}^T\mathbf{M}\right)^{-1}$ that are specified by $P^{(k)}$. Then append $\left(\left(\mathbf{M}^T\mathbf{M}\right)_{[:,R^{(k)}]}^{-1}\right)^T\mathbf{1}$ after the last column, $\left(\left(\mathbf{M}^T\mathbf{M}\right)^{-1}\mathbf{1}\right)_{R^{(k)}}$ after the last row, and $\mathbf{1}^T\left(\mathbf{M}^T\mathbf{M}\right)^{-1}\mathbf{1}$ to the left most corner to $\boldsymbol{\Phi}_{\alpha}^{(k)}$.
8. Append a zero to the last row of $\hat{\boldsymbol{\alpha}}_{R(k)}$. Calculate $\boldsymbol{\lambda}^{(k)} = \left(\boldsymbol{\Phi}_{\alpha}^{(k)}\right)^{-1}\hat{\boldsymbol{\alpha}}_{R(k)}$.
9. If all components expect the last row in $\lambda^{(k)}$ are negative, go to step 11. Otherwise, continue.
10. Find $\lambda_{\max}^{(k)} = \max_j \lambda_j^{(k)}$ and move the index in $R^{(k)}$ that corresponds to $\lambda_{\max}^{(k)}$ to $P^{(k)}$. Go to setup 7.
11. Form another matrix $\boldsymbol{\Psi}_{\lambda}^{(k)}$ by deleting every column of $\left(\mathbf{M}^T\mathbf{M}\right)^{-1}$ specified by $P^{(k)}$.
12. Let $\lambda_1^{(k)} = \lambda^{(k)}(l)$ and $\lambda_2^{(k)} = \lambda^{(k)}[1:l-1]$, where l equals to the last row of $\lambda^{(k)}$.
13. Set $\hat{\boldsymbol{\alpha}}^{(\mathrm{FCLS},k)} = \hat{\boldsymbol{\alpha}}^{\mathrm{SCLS}} - \left(\left(\mathbf{M}^T\mathbf{M}\right)^{-1}\mathbf{1}\right)\lambda_1^{(k)}\boldsymbol{\Psi}_{\lambda}^{(k)}\boldsymbol{\lambda}_2^{(k)}$. Go to step 3.

4. EXPERIMENTS

Two simulated data sets were used to substantiate the utility of MFCLS. The first data set is a set of synthetic hyperspectral images simulated by a real hyperspectral image data. The second data set is a set of synthetic Brain MR images with 0% and 20% INU corruption. Since there will be cases that both conditions could never be satisfied and causing the algorithm to run in an infinite loop, thresholds are set to safeguard this condition.

4.1 Hyperspectral Data

The idea of using synthetic images for experiments is to conduct a detailed comparative analysis on performance and computing time where the ground truth will be used to validate the results. These synthetic images to be used here were previously designed in [5] and have widely used in many research efforts. The image data used to design synthetic images is a real Cuprite image scene shown in Fig. 1(a) which is available at the USGS website http://speclab.cr.usgs.gov/cuprite.html. It is a 224-band image with size of 350×350 pixels and was collected over the Cuprite mining site, Nevada, in 1997. A total of 189 bands were used for experiments where bands 1-3, 105-115 and 150-170 have been removed prior to the analysis due to water absorption and low SNR in those bands. The ground truth available for this region provides the pixel locations of five minerals: Alunite (A), Buddingtonite (B), Calcite (C), Kaolinite (K) and Muscovite (M) shown in Fig. 1(b).

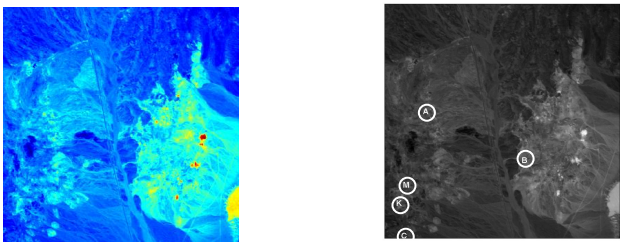

(a) (b)

Figure 1. (a) Cuprite AVIRIS image scene (b) spatial positions of five pure pixels corresponding to minerals: A, B, C, K and M

The synthetic image designed here is one of scenarios presented in [5] where the five mineral spectral signatures, A,B,C,K,M marked by circles in Fig. 1(b) were used to simulate 25 panels shown in Fig. 2 with 5 panels in each row simulated by the same mineral signature and 5 panels in each column having the same size. Among 25 panels are five 4×4 pure-pixel panels for each row in the 1st column and five 2×2 pure-pixel panels for each row in the 2nd column, the five 2×2 -mixed pixel panels for each row in the 3rd column and both the five 1×1 subpixel panels for each row in the 4th column and the 5th column where the mixed and subpanel pixels were simulated according to legends in Fig. 2. So, a total of 100 pure pixels (80 in the 1st column and 20 in 2nd column), referred to as endmember pixels were simulated in the data by the five endmembers, A,B,C,K,M.

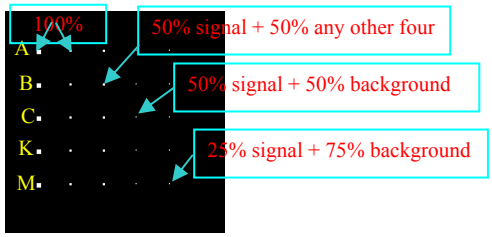

Figure 2. A set of 25 panels simulated by A,B,C,K,M

These 25 panels were then inserted in an synthetic image with size of 200×200 pixels in a way that the background pixels were removed to accommodate the inserted target pixels where the background was simulated by the sample mean of the real image scene in Fig. 1(a) corrupted by a Gaussian noise to achieve signal-to-noise (SNR) 20:1 defined in [6].

Three interesting scenarios for Target Implantation (TI), Scenario TI1, Scenario TI2 and Scenario TI3 presented in this section are designed for our experiments. The 25 panels in Fig. 2 are used as targets of interest and implanted in a synthetic image scene with size of 200×200 pixel vectors in a way that the targets to be implanted replace their corresponding background pixels. Each of these three scenarios is described as follows.

4.1.1 Scenario TI1 (Clean Panels Implanted into Clean Background)

This scenario assumes that the image background is clean and simulated by only one BKG signature. The 25 clean panels simulated in Fig. 4.2 are then implanted in the background by replacing their corresponding background pixels with the clean panel pixels. The resulting image is a synthetic image shown in Fig. 3 with clean panels implanted in the clean background image scene.

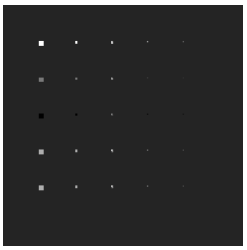

Figure 3. Synthetic image simulated by Scenario TI1

4.1.2 Scenario TI2 (Clean Panels Implanted into Noisy Background)

Practically, Scenario TI1 does not exist because of no noise present in the data. Scenario TI2 is more realistic by replacing the noise-free background in Scenario TI1 with a noisy background image which is corrupted by an additive Gaussian noise to achieve Signal-to-Noise Ratio (SNR) = 20:1. Then clean targets are implanted into such simulated noisy background image. So, the resulting synthetic image has clean targets implanted in a noisy background as shown in Fig. 4. This scenario simulates a case that true targets are indeed present in a noisy image background for target extraction.

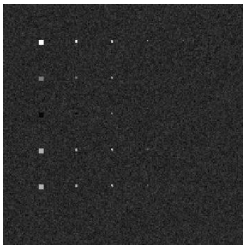

Figure 4.. Synthetic image simulated by Scenario TI2

The synthetic image scene in this scenario is the same as the one in Scenario TI1 except the image background is not clean, but rather corrupted by an additive Gaussian noise with SNR = 20:1.

4.1.3 Scenario TI3 (Gaussian Noise Added to Clean Panels Implanted into Clean Background)

Scenario TI3 is the same Scenario TI1 except that a Gaussian noise is added to TI1 to achieve an SNR = 20:1. So, in this synthetic image, the clean targets and clean background image are both corrupted by an additive Gaussian noise with SNR = 20:1 as shown in Fig. 5. It is also similar to Scenario TI2 but different in that the implanted targets are now noise-corrupted compared to the clean targets implanted in Scenario TI2.

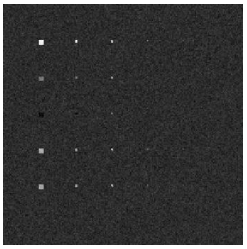

Figure 5. Synthetic image simulated by Scenario TI3

This scenario simulates a case that the implanted targets are not original true targets and have been contaminated and corrupted by noise. As a consequence of noise corruption, all the pure pixels, mixed pixels and subpixels are contaminated. So, technically speaking, those panel pixels of 100% purity as endmembers are no longer pure. However, these implanted targets are still considered to be purest and closest to the original targets compared to other pixels present in the image scene. So, they can be still considered as targets of interest. This scenario is designed to test and evaluate how sensitive a target extraction algorithm can be when clean targets are corrupted by noise.

FCLS threshold: 1e-6
MFCLS threshold: 1e-6

It should be noted that these threshold values were set to values that FCLS can converge. The processing time for TI 1-3 can be seen in the following table.

Table 1. computing time (in seconds) for simulated CUPRITE data

	TI-1	TI-2	TI-3
FCLS	0.3474	0.7766	0.7742
MFCLS	0.0061	0.0060	0.0058

From Table 1, it is obvious that with the same level of threshold, MFCLS requires less processing time in order of 10^{-3} to obtain fully abundance-constrained results. Moreover, the accuracy between FCLS and MFCLS was investigated and Fig. 6 shows the resulting mineral abundances maps.

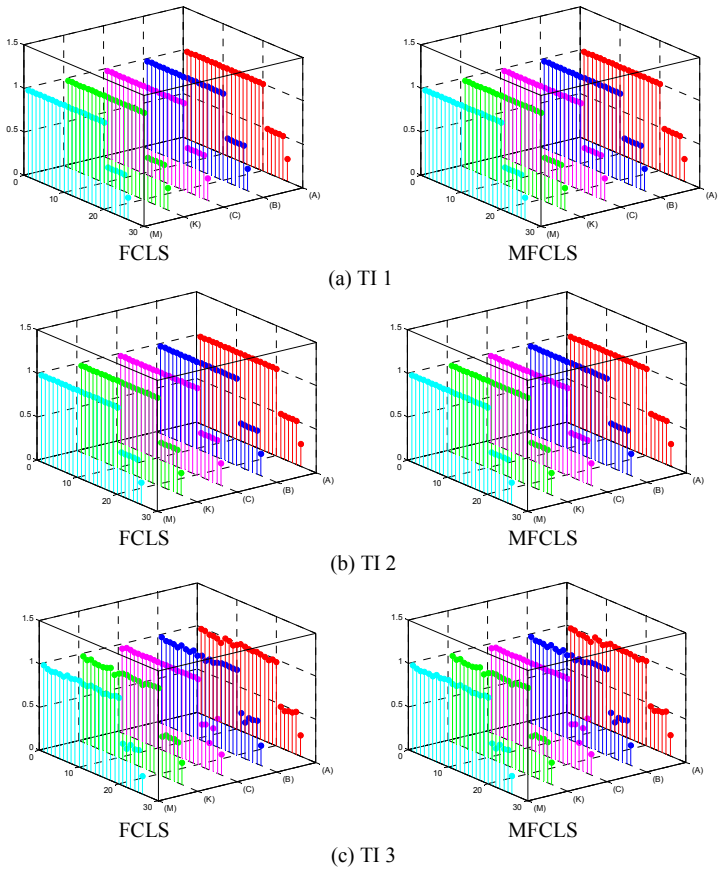

Figure 6. Abundance map of the 5 different minerals simulated for CUPRITE Hyperspectral data estimated with FCLS and MFCLS of TI-1 (a), TI-2 (b) and TI-3 (c).

By visual inspection of Fig. 6 the two methods provide very clsoe results. Furthermore, these results were analyzed with least squares error tabulated in Table 2.

Table 2. Least squares errors calculated from Fig 6.

	TI-1	TI-2	TI-3
FCLS	1.9791e-022	1.9791e-022	0.0631
MFCLS	1.0440e-021	1.0440e-021	0.0576

From Table 2, it can be seen that FCLS resulted in more accurate abundance estimation for TI 1-2. However, MFCLS was more accurate for TI 3. This suggested that MFCLS was more accurate when noise is corrupting hyperspectral data.

4.2 Magnetic Resonance Image Data

The synthetic images to be used for experiments in this section were the axial T1, T2, and proton density MR brain images (with 5-mm section thickness, 0% noise and 20% intensity non-uniformity) resulting from the MR imaging simulator of McGill University, Montreal, Canada [7]. The image volume provided separate volumes of tissue classes, such as CSF, GM, WM, bone, fat and background. The use of these web MR brain images is to allow researchers to reproduce our experiments for verification.

Fig. 7(a) shows three MR brain images with specifications provided in [7] where the 1st image is acquired by Modality = PD, Protocol = ICBM, Phantom_name = normal, Slice_thickness = 5mm, Noise = 0%, INU (intensity non-

uniformity) = 0%, the 2nd image by Modality = T1, Protocol = ICBM, Phantom_name = normal, Slice_thickness = 5mm, Noise = 5%, INU = 20% and the 3rd image by Modality = T2, Protocol = ICBM, Phantom_name = normal, Slice_thickness = 5mm, Noise = 0%, INU = 20%. Fig. 7(b) provides the ground truth also available on website [] for brain tissue substances in the images in Fig. 7(a) which will be used to verify the results obtained for our experiments.

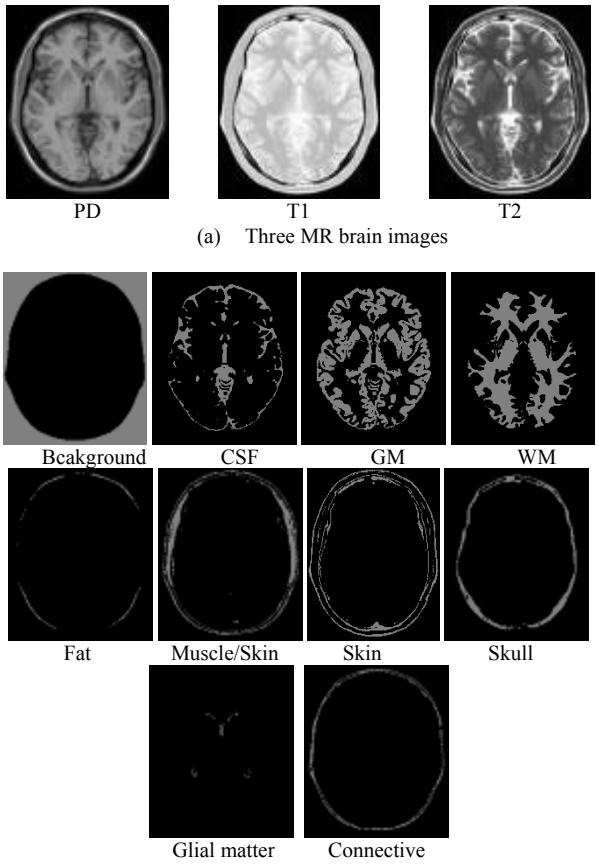

(a) Three MR brain images

Figure 7. Three MR synthetic images in (a) along with ground truth in (b)

Similar experiments conducted for synthetic hyperspectral data were also performed for the MR synthetic images where the thresholds for FCLS and MFCLS were again set to be equal to for comparison reasons and are defined as follows:

FCLS threshold: 1e-5
MFCLS threshold: 1e-5

Two different sets of MR image were experimented. One of the synthetic MR images is clean with no INU corrupted where the other is corrupted with 20% INU field. The processing time is tabulated as follows:

Table 3. Processing time (in seconds) for synthetic brain MR image experiment

	No-INU	20% INU
FCLS	7.095	7.984
MFCLS	0.000560	0.000689

As shown in Table 3, the processing time of FCLS required significantly more time that that required MFCLS in order of 10^{-4}. The classification results are shown as follows:

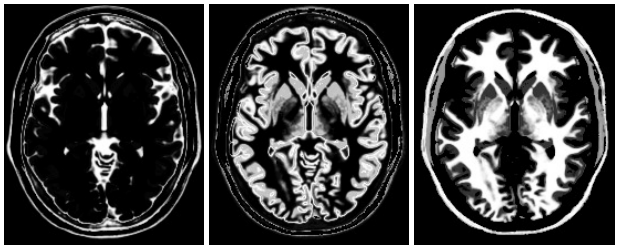

CSF GM WM

(a) 0% INU FCLS classification

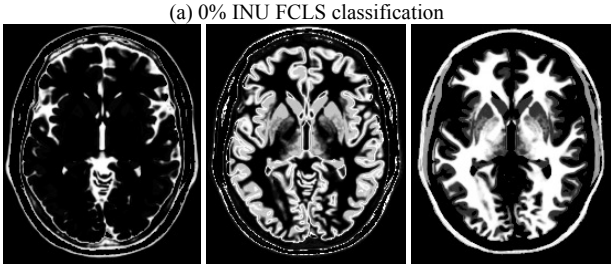

CSF GM WM

(b) 0% INU MFCLS classification

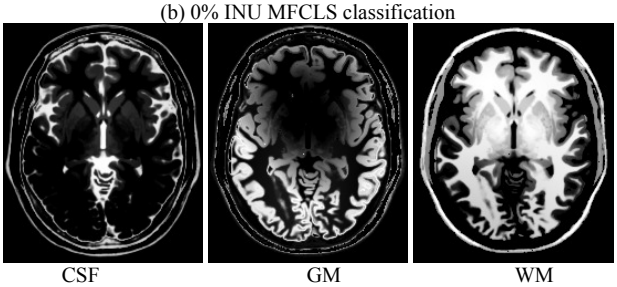

CSF GM WM

(c) 20% INU FCLS classification

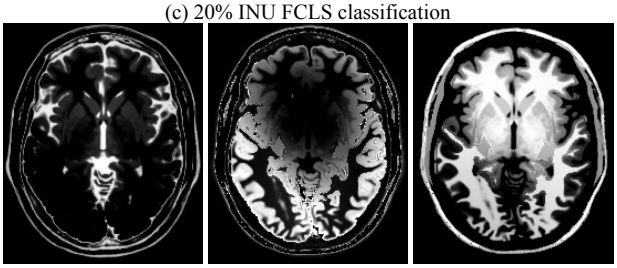

CSF GM WM

(d) 20% INU MFCLS classification

Figure 8. Synthetic brain MR image with 0% INU corruption classified with (a) FCLS and (b) MFCLS along with 20% INU corruption with (c) FCLS and (d) MFCLS classification

By visual inspection, the classification results of both 0% and 20% INU corrupted FCLS and MFCLS are very close with their least squares errors tabulated in Table 4.

Table 4. Least squares errors calculated from Fig 2.

	No-INU	20% INU
FCLS	0.0350667	0.0622276
MFCLS	0.0611285	0.0785404

According to Table 4, the FCLS estimated results are more accurate than MFCLS. However, in the 20% INU corruption case, the least squares error seems to converge between the FCLS and MFCLS results.

5. CONCLUSIONS

The MFCLS presented in this paper provides an alternative approach to FCLS where the inequality of ANC used by FCLS is replaced with an equality constraint by MFCLS. As a result, MFCLS derives two iterative equations that can be used to find optimal fully abundance-constrained solution to spectral unmixing. This is a significant advantage of using MFCLS over FCLS because MFCLS van be analyzed analytically compared to FCLS which can be evaluated by numerical algorithms. The experimental results show that both FCLS and MFCLS perform nearly the same while MFCLS requires significantly less computing time than that required by FCLS. Such a tremendous computational cost saving is a result of iterating two close forms derived by two equality constraints imposed by MFCLS. It is our brief that potential advantages of MFCLS are yet to be explored in the future.

References

1. C.-I Chang, *Hyperspectral Imaging: Techniques for Spectral Detection and Classification*, Kluwer Academic/Plenum Publishers, New York, N.Y, 2003.
2. D. Heinz and C.-I Chang, "Fully constrained least squares linear mixture analysis for material quantification in hyperspectral imagery," *IEEE Trans. on Geoscience and Remote Sensing*, vol. 39, no. 3, pp. 529-545, March 2001
3. H. Ren and C.-I Chang, "A constrained least squares approach to hyperspectral image classification," *1999 Conference on Information Science and Systems*, Johns Hopkins University, Baltimore, MD, March 17-19, 1999.
4. C.-I Chang and D. Heinz, "Constrained subpixel detection for remotely sensed images," *IEEE Trans. on Geoscience and Remote Sensing*, vol. 38, no. 3, pp. 1144-1159, May 2000.
5. C.C. Wu, C.S. Lo and C.-I Chang, "Improved process for use of a simplex growing algorithm for endmember extraction," *IEEE Trans. on Geoscience and Remote Sensing Letters*, vol. 6, no. 3, pp. 523-527, July 2009
6. J.C. Harsanyi and C.-I Chang, "Hyperspectral image classification and dimensionality reduction: an orthogonal subspace projection approach," *IEEE Trans. on Geoscience and Remote Sensing*, vol. 32, no. 4, pp. 779-785, July, 1994.
7. www.bic.mni.mcgill.ca/ brainweb/